



Geometrical structures, thermal, optical and electrical properties of azo quinoline derivatives



N.A. El-Ghamaz^a, A.A. El-Bindary^{b,*}, A.Z. El-Sonbati^b, N.M. Beshry^b

^a Physics Department, Faculty of Science, Damietta University, Damietta 34517, Egypt

^b Chemistry Department, Faculty of Science, Damietta University, Damietta 34517, Egypt

ARTICLE INFO

Article history:

Received 25 June 2015

Received in revised form 14 July 2015

Accepted 20 July 2015

Available online xxxx

Keywords:

Azo quinolines

Thermogravimetric analysis

Optical properties

Electrical properties

ABSTRACT

Azo quinoline derivatives (**AQ_x**) were synthesized by coupling of 8-hydroxyquinoline with aniline derivatives. The optimized bond lengths, bond angles and the quantum chemical parameters for the ligands (**AQ_x**) were calculated. The dielectric constants (ϵ_r and ϵ_i) and ac conductivity (σ_{ac}) were studied as a function of both temperature and frequency in the temperature range 293–509 K and frequency range 10^2 – 10^5 Hz. The thermal activation energies ΔE_1 and ΔE_2 were calculated and found to be in the range of 0.03–0.26 and 0.2–1.31 eV, respectively, depending on the substituent and frequency. The conduction mechanism was investigated for all the derivatives under investigation. The ligands (**AQ₁**, **AQ₂** and **AQ₄**) were found to be controlled by correlated barrier hopping model and the ligands (**AQ₃** and **AQ₅**) were controlled by small polaron tunneling mechanism. The optical absorption properties of the ligands thin films were investigated. The absorption coefficient (α) spectra reveals two absorption peaks which are assigned as π – π^* and n – π^* transitions. The optical energy gap (E_g) was investigated near the absorption edge and found to be in the range of 1.34–2.26 and 1.47–1.69 eV for direct and indirect optical transitions, respectively.

© 2015 Elsevier B.V. All rights reserved.

1. Introduction

The study of azo dyes has been an active area of research and attracted the attention of many researchers in recent years [1,2]. These compounds have technological, industrial and practical applications such as coloring fibers [3], optical storage technology [4] and textile dyes [5]. 8-Hydroxyquinoline derivatives and their complexes with transition metals have high antibacterial activities [6]. Also, the chemical properties of quinoline and its derivatives have been widely discussed because of their biological relevance, coordination capacity and their use as metal extracting agent [7]. They have attracted special interest due to their therapeutic properties. Quinoline azodye and its derivatives are very important compounds and have attracted much attention in both academic and applied research used in many applications such as chromophoric and metallochromic indicators in analytical chemistry [8].

The optical, electrical, thermal and structural properties of many 8-hydroxyquinoline derivatives and their metal complexes have been studied [9–14]. The dc electrical properties and conduction mechanism of azo sulfonyl quinoline ligands and their uranyl complexes have been investigated by El-Ghamaz et al. [9]. They concluded that the dc electrical conductivity (σ_{dc}) increases with increasing temperature. The thermal activation energy was found to be in the range 0.44–0.90 eV

and the dominant conduction mechanism is Variable Range Hopping mechanism (VRH). The ac conductivity and conduction mechanism of 5-(4'-derivatives phenyl azo)-8-hydroxy-7-quinolinecarboxaldehyde (**AQL_n**) and their metal complexes $[\text{Cu}(\text{AQL}_n)_2] \cdot 5\text{H}_2\text{O}$ showed semiconductor behavior with variation of temperature and according to the data, the conduction mechanisms were small polaron tunneling (SPT), quantum mechanical tunneling (QMT) and correlated barrier hopping (CBH) depending on the temperature range and type of substituent [10]. Also the thermal property investigations for **AQL_n** and $[\text{Cu}(\text{AQL}_n)_2] \cdot 5\text{H}_2\text{O}$ showed that all the complexes are thermally stable in wider temperature range than their azo ligands. The optical properties of many quinoline derivatives have been investigated by many authors [11–14]. El-Ghamaz et al. investigated the absorption and dispersion properties of different quinoline azodyes derivatives [12–14]. The electronic transition near the absorption edge of 5-(4'-derivatives phenyl azo)-8-hydroxy-7-quinolinecarboxaldehyde and Cu(II) complexes of (4-alkylphenylazo)-5-sulfo-8-hydroxyquinoline was found to be indirect allowed and the values of optical energy gap (E_g) were found in the ranges 1.33–1.92 and 2.48–3.51 eV, respectively [12,13]. The effect of substituent group variation on the optical functions, dielectric constant, optical conductivity, surface energy loss (SEL) and volume energy loss (VEL) of 5-sulfonyl-7-(4-x phenyl azo)-8-hydroxyquinoline (**SAHQ-x**) has been studied. It was found that the substitution group variation has no effect on the transmittance properties of the films in the absorption region of the spectra. Substituent variation influences the refractive index (n), the oscillator energy (E_o), the dispersion energy

* Corresponding author.

E-mail address: abindary@yahoo.com (A.A. El-Bindary).

(E_d) and the bond length of 5-Sulfo-7-(4-phenyl azo)-8-hydroxy quinoline compound [14]. M. Saçmacı et al. [11] reported that the optical transition for 2-[(E)-(8-hydroxyquinolin-5-yl)-diazonyl]-4,5-dimethoxybenzoic acid was direct allowed and has the value of 1.95 eV for energy gap.

We are interested in studying the physical properties of many quinoline ligands and their complexes because of their wide technological and industrial applications. In continuation of these studies on azo quinoline derivatives, we aimed, in present work, to investigate the optical, thermal and dielectrical properties of 5-(2-aryldiazenyl)quinolin-8-ol (AQ_x) as one of the promising azo derivatives of quinoline for many industrial and technological applications.

2. Experimental techniques

2.1. Preparation of 5-(2-aryldiazenyl)quinolin-8-ol (AQ_x)

5-(2-Aryldiazenyl)quinolin-8-ol (AQ_x) ligands are prepared according to El-Sonbati et al. [15,16]. In a typical preparation, 25 ml of distilled water containing 0.01 mol hydrochloric acid is added to aniline (0.01 mol) or its *p*-derivatives. A solution of 0.01 mol sodium nitrite in 20 ml of water is added dropwise to the resulting mixture then stirred and cooled to 0 °C. The formed diazonium chloride is consecutively coupled with an alkaline solution of 0.01 mol quinolin-8-ol, in 10 ml of pyridine. The preparation of ligands (AQ_x) is summarized in Scheme S1 in the supplementary. The colored precipitate, which formed immediately, is filtered through sintered glass crucible and washed several times with water. The crude products are purified by recrystallization from hot ethanol and dried in vacuum desiccator over P_2O_5 . Yield percent was 65–81%. The ligands are also characterized by IR spectroscopy.

The resulting formed ligands (AQ_x) are:

- AQ_1 : 5-(2-(4-methoxyphenyl)diazenyl)quinolin-8-ol.
- AQ_2 : 5-(2-(4-methylphenyl)diazenyl)quinolin-8-ol.
- AQ_3 : 5-(2-phenyldiazenyl)quinolin-8-ol.
- AQ_4 : 5-(2-(4-chlorophenyl)diazenyl)quinolin-8-ol.
- AQ_5 : 5-(2-(4-nitrophenyl)diazenyl)quinolin-8-ol.

2.2. Preparation of azo thin films

Homogenous thin films of (AQ_x) are prepared by a conventional spin coating technique onto pre-cleaned optical flat quartz substrates [17]. The prepared ligands are dissolved in chloroform until saturation. The rotating speed of the spin coating system is controlled to be about 1600 rps. The thicknesses of the prepared thin films are then measured optically by the Michelson interferometric method [18]. The measured thicknesses of the prepared thin films are found to be in the range 400–500 nm.

2.3. Analytical techniques

The infrared spectra are recorded as KBr discs using a Jasco FTIR-4100 spectrophotometer. The 1H -NMR spectra by Bruker WP 300 MHz using $DMSO-d_6$ as a solvent containing TMS as the internal standard. Mass spectra were recorded by the EI technique at 70 eV using MS-5988 GS-MS Hewlett-Packard. Ultraviolet-visible (UV-vis) spectra of the compounds are recorded in the wavelength range 200–900 nm using a Perkin-Elmer AA800 spectrophotometer Model AAS. X-ray diffraction measurement (XRD) is recorded on X-ray diffractometer in the range of diffraction angle $2\theta^\circ = 5-80^\circ$. This analysis is carried out using $CuK\alpha_1$ radiation ($\lambda = 1.540598 \text{ \AA}$). The applied voltage and the tube current are 40 KV and 30 mA, respectively. The diffraction peaks are indexed and the lattice parameters are determined with the aid of CRYSFIRE computer program [19]. Thermal analysis of the ligands are carried out using a Shimadzu thermogravimetric analyzer under nitrogen atmosphere

with heating rates of 10–15 °C/min over a temperature range from room temperature up to 1073 K. The molecular structures of the investigated compounds are optimized by HF method with 3–21 G basis set. The molecules are built with the Perkin Elmer ChemBio Draw and optimized using Perkin Elmer ChemBio3D software [20,21].

The ac conductivity measurements are performed on the samples in the form of discs of thickness 0.3–0.8 mm and compressed under a pressure of 4 t cm^{-2} using hydraulic press. The ac conductivity measurements of samples are measured as a function of temperature in the range 293–509 K and frequency range 10^2-10^5 Hz using Stanford research systems Model SR 720 LCR METER. The capacitance (C_p) and the loss tangent ($\tan \delta$) are measured in parallel mode. The temperature is measured by NiCr–NiAl thermocouple. The potential across the heater varied gradually through a variac transformer to produce a slow rate of increase of temperature in order to obtain accurate temperature measurements. The range of temperature for electrical measurements is chosen according to TGA measurements.

3. Results and discussion

3.1. Molecular structures of the ligands

The calculated molecular structures for ligands (AQ_x) are shown in Fig. 1. Primary calculations reveal that the azo form (**B**) is more stable and reactive than azo form (**A**) (Scheme S1 in the supplementary). The calculated quantum chemical parameters are listed in Table 1. Molecular structures (HOMO & LUMO) are presented in Fig. S1 in the supplementary for ligands (AQ_x) [azo form (**B**)]. Selected geometric parameter bond lengths and bond angles of AQ_x are tabulated in Tables S1–S5 in the supplementary for ligands (AQ_x) [azo form (**B**)]. The HOMO–LUMO energy gap (E_t) is an important stability index which is applied to develop theoretical models for explaining the structure and conformation barriers in many molecular systems. As the value of E_t decreases the stability of the compound increases [17, 20,21]. Additional parameters such as separation energies (E_i), absolute electronegativities (χ), chemical potentials (P_i), absolute hardness (η), absolute softness (σ), global electrophilicity (δ), global softness (S_g) and additional electronic charge (ΔN_{max}) are calculated according to the following equations [17,20,21]:

$$E_t = E_{LUMO} - E_{HOMO} \quad (1)$$

$$\chi = \frac{-(E_{HOMO} + E_{LUMO})}{2} \quad (2)$$

$$\eta = \frac{E_{LUMO} - E_{HOMO}}{2} \quad (3)$$

$$\sigma = 1/\eta \quad (4)$$

$$P_i = -\chi \quad (5)$$

$$S_g = \frac{1}{2\eta} \quad (6)$$

$$\delta = P_i^2/2\eta \quad (7)$$

$$\Delta N_{max} = -P_i/\eta. \quad (8)$$

The values of E_t for AQ_1 , AQ_2 , AQ_3 , AQ_4 and AQ_5 ligands were found 2.386, 2.576, 2.696, 2.327 and 3.135 eV, respectively.

3.2. IR spectra of the ligands

All of the free ligands showed IR characteristic bands at 1555, 1540 and 3200 cm^{-1} assigned to $\nu(C=N)_{py}$, $\nu(-=N-)$ and $\nu(OH)$

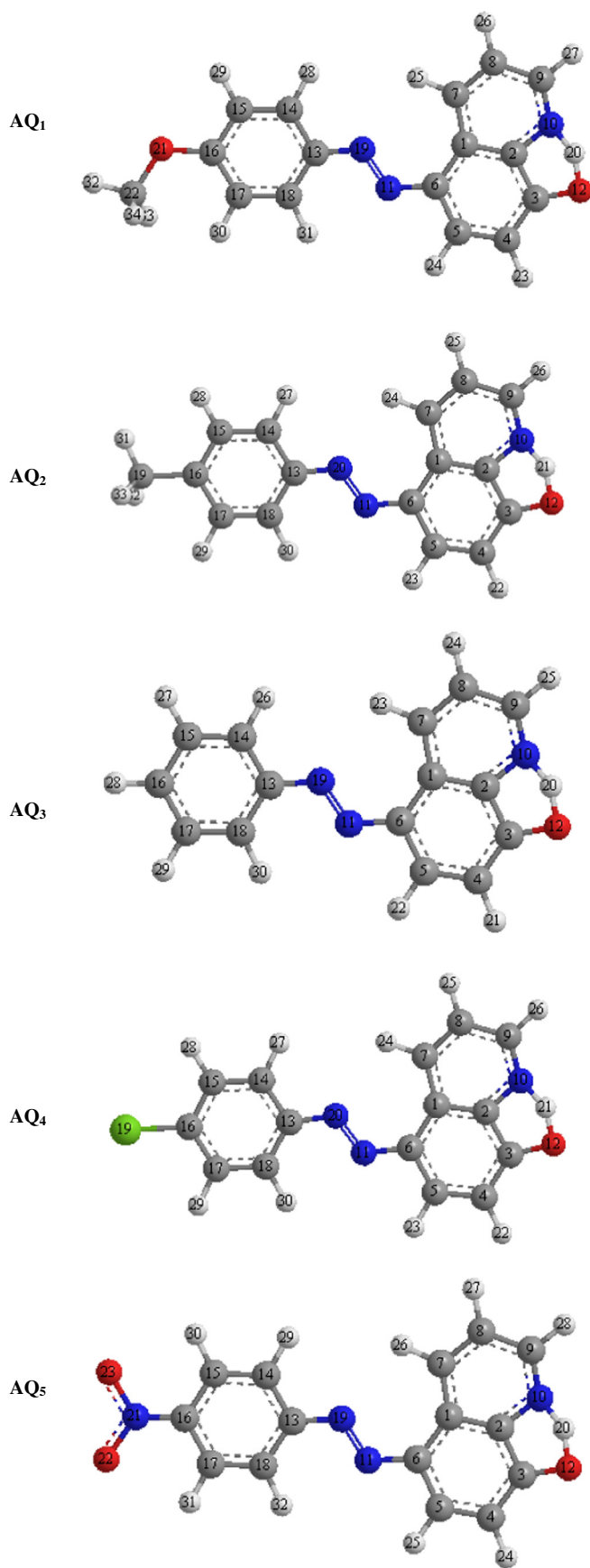


Fig. 1. The calculated molecular structures of the investigated compounds (AQ_x).

frequencies, respectively. El-Sonbati and co-workers [22–24] found three kinds of OH structures on the basis of the IR frequencies:

- (i) Only oxygen is in the bridge while the hydrogen is free.
- (ii) Polymer chains are formed in which both hydrogen and oxygen atoms are precipitating in the hydrogen bond.
- (iii) Dimer associated structures are formed.

On the basis of these, AQ_x exists on a five-membered chelate skeleton and the hydrogen bonding could be classified into two types:

- (a) Intramolecular hydrogen bonding O–H...N (Scheme S1(B) in the supplementary) resulted from hydrogen (C_8 –OH) and nitrogen of azomethine group ($C=Npy$).
- (b) Intermolecular hydrogen bonding O–H...O (Scheme S1(C) in the supplementary) and (O–H...N) (Scheme S1(D) in the supplementary) resulted from the C_8 –OH group through two molecules and/or C_8 –OH with $C=N$ through two molecules.

The assignment of the $C=N$ and $C-C$ stretching modes on our previous work [23,24] and investigations by Henry et al. has been reported [25]. Upon comparing the position of these bands for different ligands, it was found that ring substitution resulted in a shift to lower frequencies. This behavior can probably be explained by the lowering in the electronic density caused by electronegative groups.

These comparisons showed that the electronegativity of the ring substituents produces not only a decrease in the electronic density over the ring, geometrating a diminution in the $\nu(C=N)$ stretching frequency, but also causes a plane deformation, doubly degenerate stretch and doubly degenerate in plane bending in D_{3h} symmetry [26].

3.3. Mass spectra

The electron impact mass spectrum of ligand (AQ_3) is recorded and investigated at 70 eV of electron energy. The mass spectrum fragmentation mode of ligand (AQ_3) shows the exact mass of 249 corresponding to the formula $C_{15}H_{11}N_3O$. The ion of $m/z = 249$ undergoes fragmentation to a stable peak at $m/z = 172$ by losing C_6H_5 atoms (structure I) as shown in Scheme 1. The loss of N_2 leads to the fragmentation with $m/z = 144$ (structure II). The loss of CHO atoms leads to the fragmentation with $m/z = 115$ (structure III). A breakdown of the backbone of AQ_3 ligand gives the fragment (IV).

3.4. 1H NMR spectra

The 1H NMR spectra of the free ligands (AQ_x) in DMSO- d_6 showed two signals in the range 8.95–9.30 ppm. These signals are probably assigned to the azomethine group and hydroxy group of 8-hydroxyquinoline derivatives [23]. The presence of these signals at high values downfield of TMS is due to hydrogen bonding between this hydroxy group and the nitrogen of azo group. We also found that upon deuteration of the solution the signal disappeared.

3.5. X-ray diffraction analysis

Single crystals of the ligands could not be prepared to get the XRD and hence the powder diffraction data were obtained for structural characterization. Structure determination by X-ray powder diffraction data has gone through a recent surge since it has become important to get to the structural information of materials, which do not yield good quality single crystals. The X-ray diffraction (XRD) pattern of AQ_3 ligand in powder form is shown in Fig. 2. The XRD pattern shows that AQ_3 ligand has a polycrystalline nature. The calculated crystal system is found to be monoclinic with space group P21/A. The estimated lattice parameters are found to be 20.4710 Å, 18.8150 Å, 19.9590 Å, 90.0°, 92.7° and 90.0° for a, b, c, α , β and γ , respectively. The inter-planar

Table 1
The calculated quantum chemical parameters for the investigated compounds (**AQ_x**).

Compound	E _{HOMO} (eV)	E _{LUMO} (eV)	E _t (eV)	X (eV)	η (eV)	σ (eV) ⁻¹	Pi (eV)	S (eV) ⁻¹	ω (eV)	ΔN _{max}
AQ₁										
Form A	-4.694	-2.038	2.656	3.366	1.328	0.753	-3.366	0.377	4.266	2.535
Form B	-4.079	-1.695	2.386	2.887	1.192	0.839	-2.887	0.419	3.497	2.422
AQ₂										
Form A	-4.897	-2.035	2.862	3.466	1.432	0.699	-3.466	0.349	4.197	2.421
Form B	-4.266	-1.689	2.576	2.978	1.288	0.776	-2.978	0.388	3.442	2.312
AQ₃										
Form A	-5.021	-2.030	2.991	3.525	1.495	0.669	-3.525	0.334	4.156	2.358
Form B	-4.384	-1.684	2.696	3.034	1.349	0.741	-3.034	0.370	3.410	2.248
AQ₄										
Form A	-4.615	-2.029	2.586	3.322	1.293	0.773	-3.322	0.387	4.267	2.569
Form B	-4.011	-1.684	2.327	2.847	1.164	0.859	-2.847	0.429	3.484	2.447
AQ₅										
Form A	-6.381	-2.735	3.646	4.558	1.823	0.549	-4.558	0.274	5.698	2.500
Form B	-5.573	-2.438	3.135	4.006	1.567	0.638	-4.006	0.319	5.118	2.556

spacing (*d*) and Miller indices (*hkl*) which are estimated by CRYSFIRE are listed in Table 2. The average crystallite size (*S*) is calculated according to Scherer's equation [27,28] as follows:

$$S = \frac{0.95\lambda}{\psi \cos \theta} \quad (9)$$

where ψ is the width measured in radians of the half-maximum peak intensity, λ is the X-ray wavelength and θ is the Bragg's angle. The estimated crystallite size (*S*) is found to be about 24.3 nm.

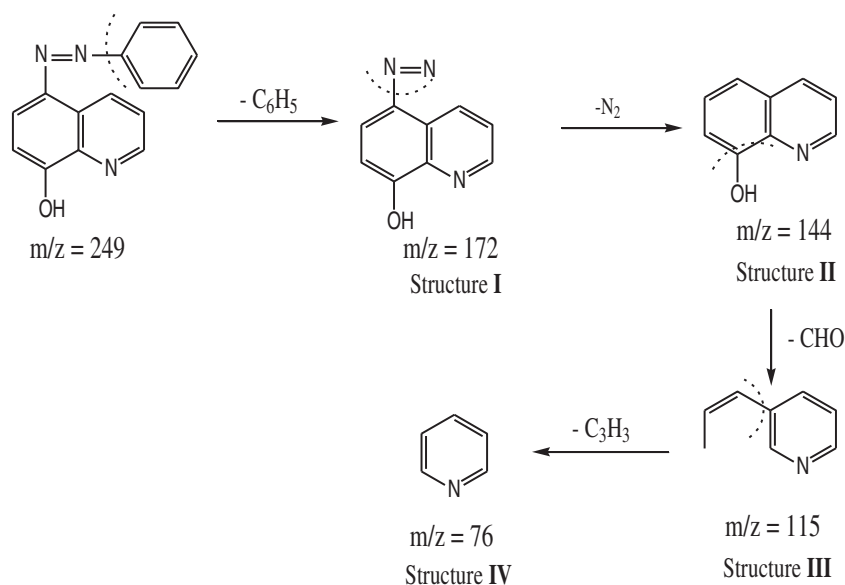
3.6. Thermal analysis

The TGA data for **AQ₂**, **AQ₃** and **AQ₅** shows two steps of the loss of masses, while for **AQ₁** and **AQ₄** shows three steps. The loss of about ~4% of **AQ₅** at the first heating stage up to 50 °C may be due to loss of moisture. The temperature intervals and the percentage of loss of masses corresponding to the probable decomposition processes are listed in Table 3.

The TGA is used for the determination of rates of decomposition of **AQ_x**. The rate constant of the thermal decomposition is plotted according to the Arrhenius relationship [21]:

$$\ln K^* = \ln \beta - \frac{E^*}{RT}, \quad (10)$$

where K^* is the rate constant of the thermal decomposition, β is a pre exponential constant, E^* the thermal activation energies of decomposition, R is a gas constant ($8.314 \text{ J} \cdot \text{mol}^{-1} \cdot \text{K}^{-1}$) and T is the absolute temperature. The values of E^* are calculated from the slope of the straight line obtained from the plot $\ln K^*$ versus $1/T$ as shown in Fig. 3. The values of E^* are found to be 76.09, 73.27, 78.61, 85.68 and 88.86 kJ/mol for **AQ₁**, **AQ₂**, **AQ₃**, **AQ₄** and **AQ₅**, respectively. The high values of the activation energies (E^*) reflect the thermal stability of the compounds. So, it is clear from TGA analysis that **AQ₅** ligand is more stable than the other ligands [27]. This can be attributed to the fact that the effective charge experienced increases by the electron withdrawing *p*-substituent -Cl and -NO₂ (**AQ₄** and **AQ₅**) while it decreases by the electron donating



Scheme 1. Fragmentation patterns of **AQ₃** ligand.

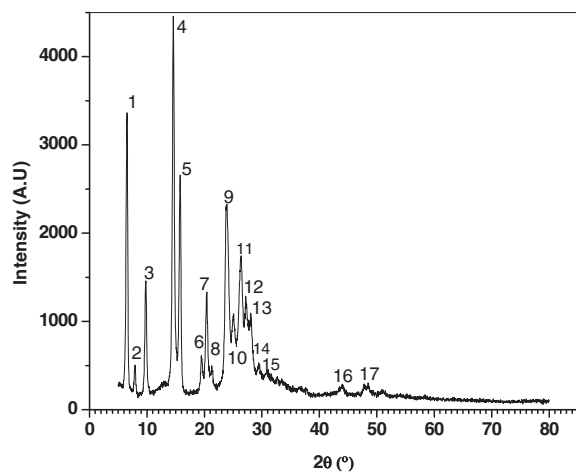


Fig. 2. X-ray diffraction pattern of AQ_3 in the powder form.

character of $-OCH_3$ and $-CH_3$ (AQ_1 and AQ_2). This is in accordance with that expected from Hammett's constant (σ^R) as shown in Fig. 4.

3.7. Optical properties of 5-(2-(aryldiazenyl)quinolin)-8-ol (AQ_x) thin films

Valuable information about the energy band structure and the most probable electronic transition can be extracted from the absorption spectra of a material in accordance to the Orbital Molecular Theory. The absorption coefficient (α) is calculated from the measured absorbance (*Abs.*) according to the following equation [29]:

$$\alpha = \frac{2.3Abs.}{L}, \quad (11)$$

where L is the thickness of the film.

The absorption coefficient (α) of AQ_x thin films as a function of incident photon energy ($h\nu$) is shown in Fig. 5. The absorption coefficient spectrum revealed two peaks indicating transitions of charge carriers from bonding to antibonding molecular orbitals. The bands appearing at 3.0–3.5 eV are assigned to $n-\pi^*$ transitions of azodye derivatives function group $N=N$ [30]. The bands appearing at 5.0–5.2 eV are

Table 3
The thermal analysis data for ligands (AQ_x).

Compound	Temp. range (°C)	Found mass loss (calc.)%	Assignment
AQ_1	50–136	11.8 (11.11)	Loss of OCH_3
	136–300	44.5 (43.01)	Loss of $C_6H_4N_2O$
	300–800	40.3 (41.57)	Loss of C_8H_6N
	>800	3.39 (4.30)	Loss of C atom
AQ_2	90–300	63.64 (65.40)	Loss of $C_9H_6N_3O$
	300–800	27.50 (25.48)	Loss of C_5H_7
	>800	8.86 (4.56)	Loss of C atom
AQ_3	100–300	48.10 (48.59)	Loss of $C_6H_5N_2O$
	300–800	47.40 (46.59)	Loss of C_8H_6N
	>800	4.50 (4.82)	Loss of C atom
	AQ_4	110–300	66.55 (67.55)
AQ_4	300–430	10.96 (9.88)	Loss of N_2
	430–800	18.04 (18.34)	Loss of C_4H_4
	>800	4.45 (4.23)	Loss of C atom
	AQ_5	120–270	56.51 (56.46)
270–800		36.79 (39.46)	Loss of C_8H_6N
>800		6.70 (4.08)	Loss of C atom

assigned to $\pi-\pi^*$ transitions between orbitals largely localized in phenyl ring [30].

The energy gap value and the type of optical transition can be obtained from the data of α near the absorption edge using the following relation [31,32]:

$$\alpha h\nu = B(h\nu - E_g \pm E_{ph})^x, \quad (12)$$

where B is a constant, which depends on the electronic transition probability [33], E_g is the optical energy gap of the material and E_{ph} is the energy of phonon accompanying the indirect transition (the factor \pm allows for the possibility of photon absorption or emission, with the +ve sign corresponding to absorption and the -ve sign to emission) and x is the power which characterizes the transition process, where $x = 1/2$ and $3/2$ for direct allowed and forbidden transitions, respectively, and $x = 2$ and 3 for indirect allowed and forbidden transitions, respectively. The dependence of the optical absorption of an incident phonon energy is examined in terms of Eq. (12) and we found that the best fit of the experimental data of α near the absorption edge is for the value of $x = 3/2$ for all ligands and $x = 2$ for AQ_1 and AQ_4 . This indicates that the forbidden direct transition is the probable electronic transition for all ligands, on the other hand, the indirect allowed transition is also probable for the ligands AQ_1 and AQ_4 . The dependence of $(\alpha h\nu)^{1/2}$ and $(\alpha h\nu)^{2/3}$ on incident photon energy is presented in

Table 2
Crystallographic data of AQ_3 ligand.

Peak no.	$2\theta_{obs.}$ (°)	$d_{obs.}$ (Å)	$d_{cal.}$ (Å)	(hkl)
1	6.514	13.56162	13.70641	0 1 1
2	7.917	11.16377	11.21252	1 1 1
3	9.788	9.030481	8.988331	$\bar{2}$ 1 0
4	14.586	6.070134	6.070134	$\bar{1}$ 1 3
5	15.772	5.614431	5.606259	2 2 2
6	19.490	4.5526	4.563389	0 3 3
7	20.388	4.354438	4.344614	4 1 2
8	21.288	4.170547	4.170547	3 2 3
9	23.871	3.724855	3.730266	$\bar{4}$ 3 2
10	24.110	3.689176	3.692713	$\bar{2}$ 3 4
11	25.052	3.553044	3.562905	$\bar{5}$ 2 2
12	26.359	3.378509	3.385934	$\bar{3}$ 4 3
13	27.205	3.276478	3.275085	0 5 3
14	28.082	3.175185	3.176495	3 2 5
15	29.584	3.017235	3.0196	3 4 4
16	44.022	2.055778	2.055778	$\bar{7}$ 6 3
17	47.760	1.902915	1.902915	$\bar{5}$ 8 4

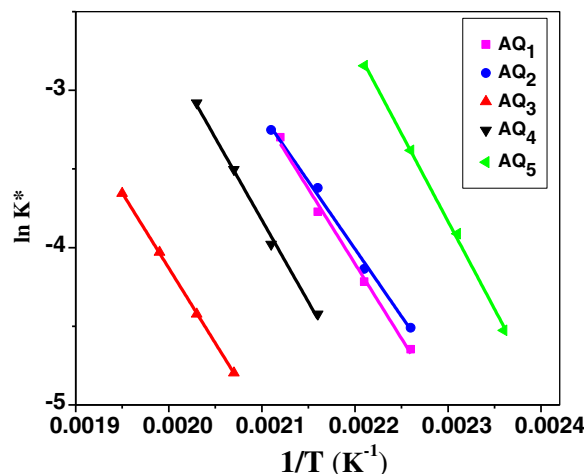


Fig. 3. The relation between $\ln K^*$ and $1/T$ for AQ_x .

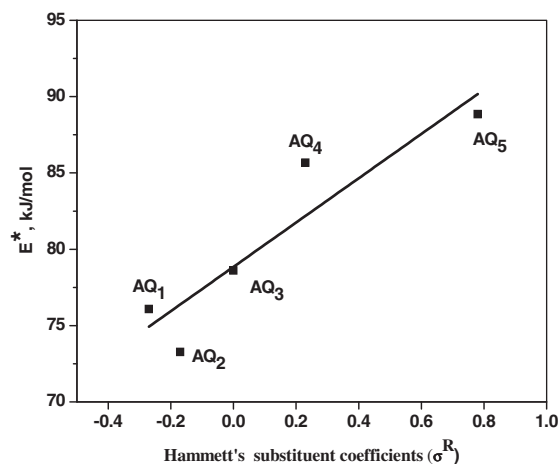


Fig. 4. The relation between thermal activation energies of decomposition (E^*) and Hammett's substituent coefficients (σ^R) for AQ_x .

Figs. 6 and 7, respectively. The intersection of extrapolation of the linear part to zero absorption with photon energy axes is taken as the fundamental energy gap. The determined values of E_g and E_{ph} are listed in Table 4. The variation of the obtained values of E_g and the type of the electronic transition may be attributed to either withdrawing or donating function group [13]. The effect of methoxy group is reducing the E_g value this is because of the methoxy group is a strong donating function group, while the effect of halogen group as withdrawing function group is to raise the E_g . A similar effect of the substituent OCH_3 is reported by Leontie and Danac [34]. The values of HOMO–LUMO energy gap (E_t) are found to exceed the optical energy gap (E_g). Similar results were obtained for antipyrine Schiff base derivatives [17] and other π -conjugated organic molecules such as α -sixithiophene (α -6 T), N,N' -diphenyl- N,N' -bis(L-naphthyl)-1,1'-biphenyl-4,4'' diamine (α -NPD), tris(8-hydroxy-quinoline)aluminum (Alq_3) and 3,4,9,10-perylene-tetracarboxylic dianhydride (PTCDA) [35]. The value of ($E_t - E_g$) is considered as the binding energy of excites [35] and found to be in the range 0.3–1.0 eV for AQ_x .

3.8. AC measurements analysis

The dielectric constant (ϵ) is considered as a complex quantity and given by the equation:

$$\epsilon = \epsilon_r - i\epsilon_i, \tag{13}$$

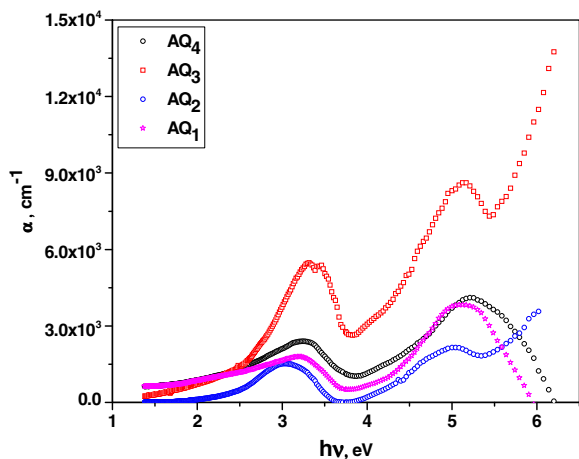


Fig. 5. The absorption coefficient (α) as a function of the incident photon energy $h\nu$ for AQ_x thin films.

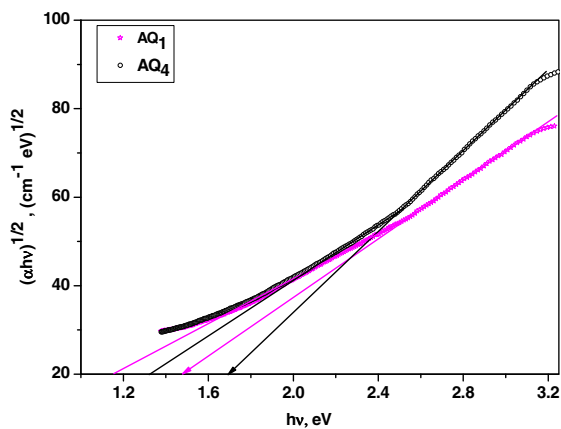


Fig. 6. Plot of $(\alpha h\nu)^{1/2}$ vs. $h\nu$ for AQ_n thin films.

where ϵ_r is the real part of the dielectric constant and ϵ_i is the imaginary part of the dielectric constant. The real dielectric constant (ϵ_r) can be calculated from the parallel mode measured capacitance by the equation [36,37]:

$$\epsilon_r = \frac{C_p L}{\epsilon_0 A}, \tag{14}$$

where C_p is the capacitance of the samples measured in parallel mode, ϵ_0 is the permittivity of free space, A is the cross sectional area and L is the thickness of the samples. The imaginary part of the dielectric constant (ϵ_i) can be calculated from the calculated values of ϵ_r and the measured values of loss tangent ($\tan \delta$) using the equation [36,37]:

$$\epsilon_i = \epsilon_r \tan \delta. \tag{15}$$

The value of ϵ_r and ϵ_i are calculated. The temperature dependence of ϵ_r and ϵ_i at different frequencies is shown in Figs. 8 and 9, respectively. In general, both of ϵ_r and ϵ_i , decrease with increasing frequency and increase with increasing temperature for all ligands (AQ_x). This behavior is in agreement with the expected behavior of the organic materials [12,36].

The ac conductivity (σ_{ac}) for AQ_x derivatives were calculated from the calculated values of ϵ_i according to the following equation [36]:

$$\sigma_{ac} = \omega \epsilon_0 \epsilon_i, \tag{16}$$

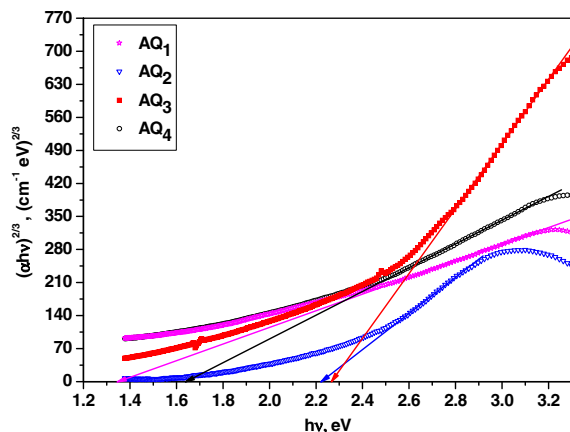


Fig. 7. Plot of $(\alpha h\nu)^{2/3}$ vs. $h\nu$ for AQ_x thin films.

Table 4
Optical energy gaps of the investigated ligands **AQ_x**.

Compound	$E_g^{ind.}$ (eV)	E_{ph} (eV)	$E_g^{dir.}$ (eV)
AQ₁	1.47	0.16	1.34
AQ₂	–	–	2.21
AQ₃	–	–	2.26
AQ₄	1.69	0.18	1.64

where ω is the angular frequency of applied field ($\omega = 2\pi f$ (where f is the frequency)). The calculated values of σ_{ac} for the **AQ_x** under consideration as a function of temperature are investigated in the

temperature and frequency ranges considered before and are shown in Fig. 10. The values of σ_{ac} increases with increasing frequencies as expected, while the behavior of σ_{ac} with increasing temperature depends on the chemical composition of each ligand and the decomposition stages observed in the TGA measurements. The conductivity of **AQ₁**, **AQ₂**, **AQ₄** and **AQ₅** ligands, shown in Fig. 10, increases gradually with increasing temperature until the decomposition process starts.

The ac electrical conductivity (σ_{ac}) as a function of temperature is given by equation [12,36,37]:

$$\sigma_{ac} = \sigma_0 \exp\left(\frac{-\Delta E}{k_B T}\right), \quad (17)$$

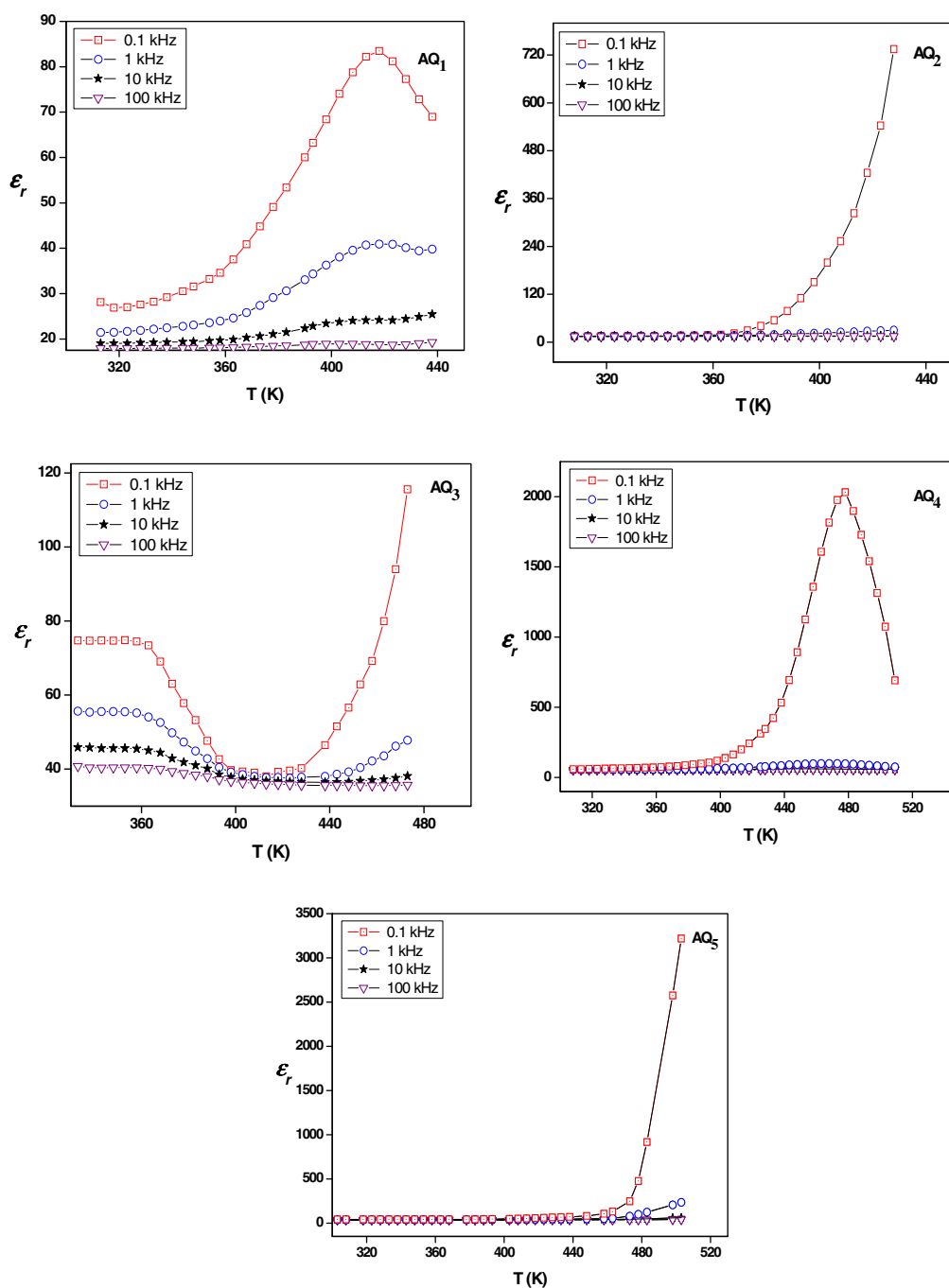


Fig. 8. Temperature and frequency dependence of the real dielectric constant (ϵ_r) for ligands (**AQ_x**).

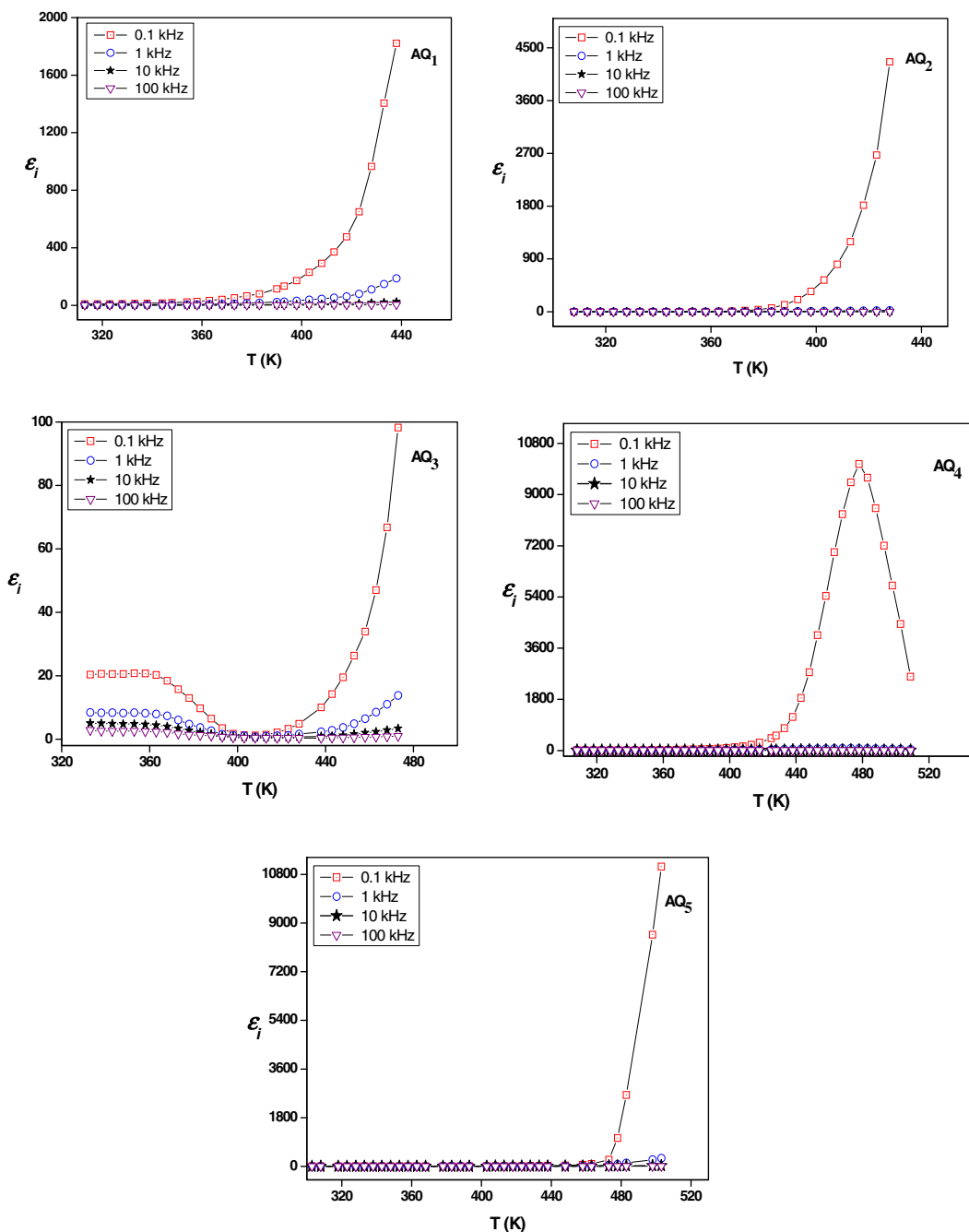


Fig. 9. Temperature and frequency dependence of the imaginary dielectric constant (ϵ_i) for ligands (AQ_x).

where σ_0 is the pre-exponential constant, ΔE is the thermal activation energy and k_B is Boltzmann's constant. The relation between $\ln \sigma_{ac}$ as a function of $(1/T)$ for AQ_x is shown in Fig. 11 in the temperature and frequency ranges under consideration. The semiconductor behavior observed in these figures is characterized by two thermal activation energies (ΔE_1 and ΔE_2) depending on the temperature range. The values of the thermal activation energy, ΔE_1 and ΔE_2 , for AQ_x at different frequencies are determined in the low and high temperature regions, respectively, and listed in Table 5. The variation in the values of ΔE_1 and ΔE_2 is due to the effect of the substituents [12,36]. The relatively low values of ΔE_1 for all ligands at all test frequencies suggested that the operating conduction mechanism may be tunneling and/or hopping. The relatively high values of ΔE_2 in the higher region of temperature

suggest the conduction mechanism to be thermally activated process. It is found that AQ_5 has the lowest values for ΔE_1 and ΔE_2 . The lower and upper limits of ΔE_1 at test frequency 0.1 kHz are found to be 0.03, 0.19 eV for AQ_5 and AQ_1 , respectively, while those of ΔE_2 are found to be 0.33, 1.31 eV for AQ_5 and AQ_2 , respectively.

To investigate the suitable operating conduction mechanism, theoretical model has been reported to correlate the conduction mechanism with the behavior of σ_{ac} with the frequency [12,36,37]. The frequency dependence of σ_{ac} at certain temperature can be investigated according to the equation [36–38]:

$$\sigma_{ac} = A^* \omega^s, \tag{18}$$

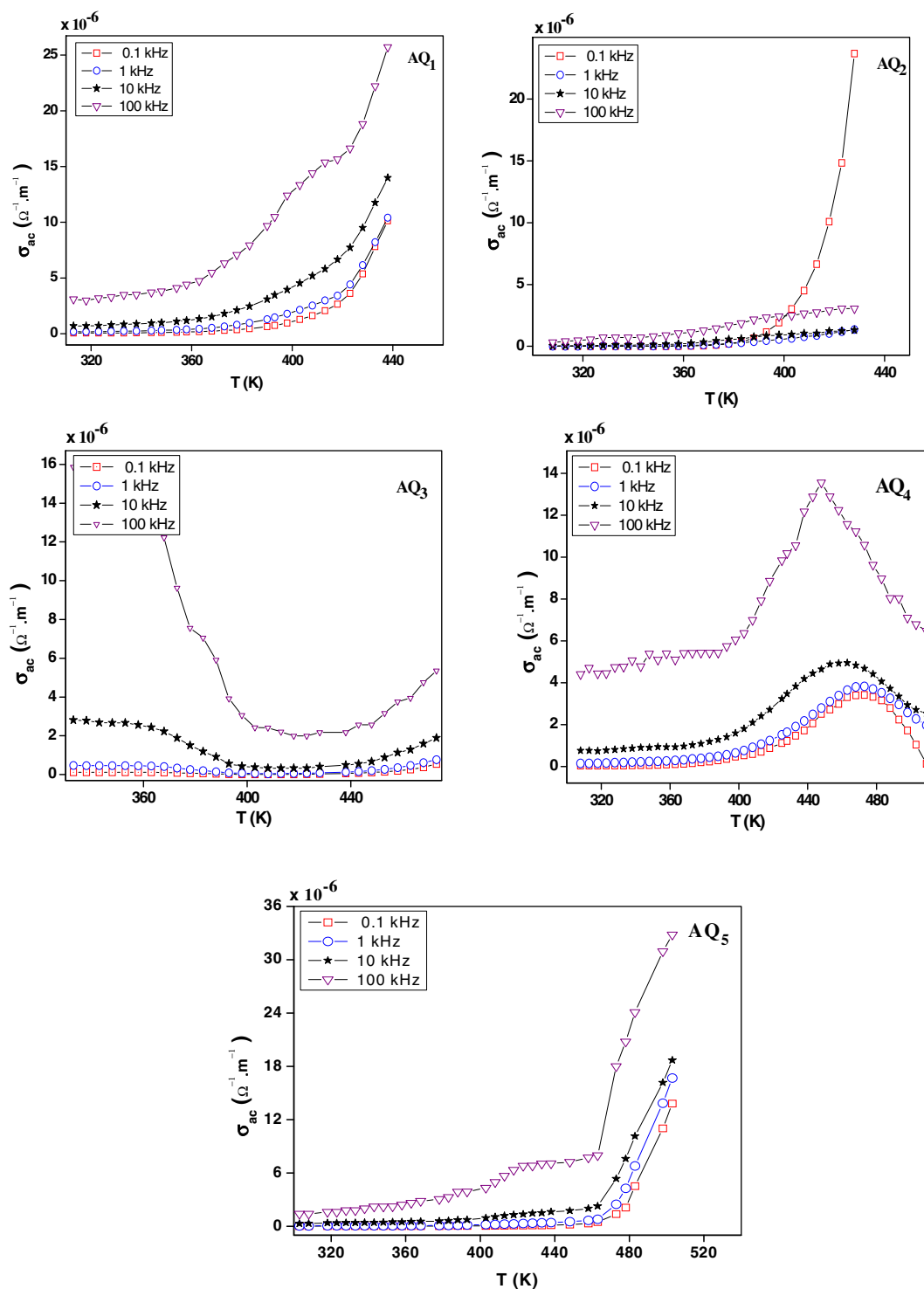


Fig. 10. The conductivity (σ_{ac}) as a function of temperature for ligands (AQ_x) at different test frequencies.

where A^* is a constant depending on temperature, ω is the angular frequency and S is an exponent in which its value and its behavior with temperature determines the dominant conduction mechanism. The value of S is the slope of the straight line obtained from the relation between $\log \sigma_{ac}$ and $\log \omega$. The values of S as a function of temperature for AQ_x are shown in Fig. 12. The general behavior of S with temperature for AQ_1 , AQ_2 and AQ_4 appears to be consistent with the hopping process of charge carriers between localized sites

and suggested that the correlated barrier hopping (CBH) model is the best suitable model for conduction mechanism [12,36,37], while small polaron tunneling (SPT) model is found to be more suitable with AQ_3 and AQ_5 . In SPT model the ac conductivity is given by following equation [39,40]:

$$\sigma_{ac(SPT)} = \frac{\pi^4 e^2 K_B T [N(E_F)]^2 \omega R_W^4}{24 \alpha} \quad (19)$$

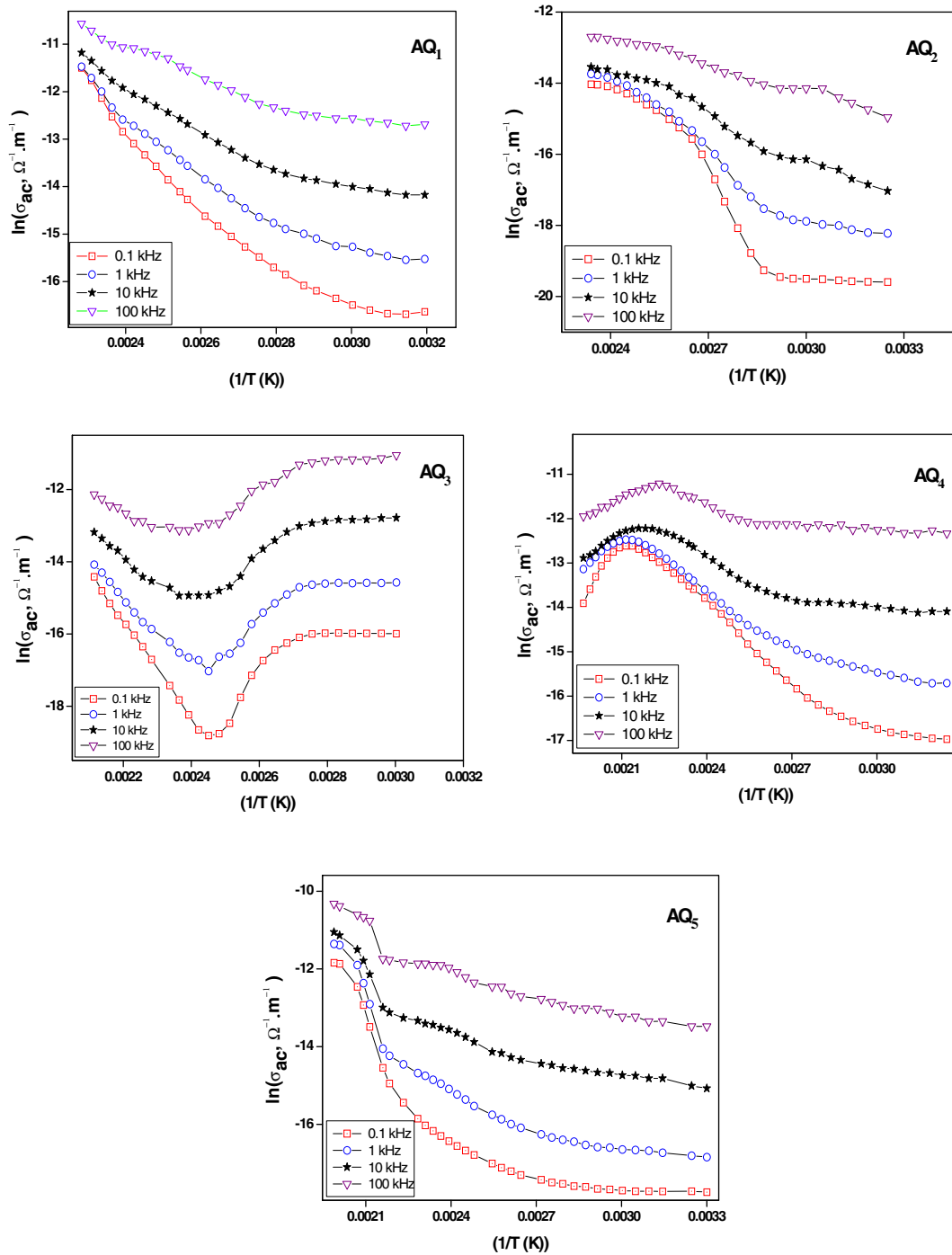


Fig. 11. $\ln \sigma_{ac}$ vs. $1/T$ for ligands (AQ_x) at different test frequencies.

Table 5

Thermal activation energies (ΔE_1 and ΔE_2) for the ligands (AQ_x).

Compound	ΔE_1 (eV)				ΔE_2 (eV)				
	0.1 kHz	1 kHz	10 kHz	100 kHz	0.1 kHz	1 kHz	10 kHz	100 kHz	0.1 kHz
AQ_1	0.19	0.15	0.1	0.06	0.58	0.48	0.38	0.31	0.58
AQ_2	0.05	0.15	0.26	0.22	1.31	0.82	0.54	0.27	1.31
AQ_3	–	–	–	–	1.13	0.75	0.57	0.31	1.13
AQ_4	0.15	0.12	0.04	0.03	0.49	0.43	0.33	0.25	0.49
AQ_5	0.03	0.06	0.08	0.09	0.33	0.35	0.26	0.2	0.33

where α is the spatial extent of polaron, $N(E_F)$ the density of states at the Fermi level and R_w is the tunneling distance. According to this model, the frequency exponent (S) is evaluated as,

$$S = 1 - \frac{4}{\ln[1/\omega\tau_0] - W_H/T}, \tag{20}$$

where W_H is the barrier height for infinite site separation. In CBH model the ac conductivity is given by following equation [39,40]:

$$\sigma_{ac(CBH)} = \frac{n\pi^3}{24} N^2 \epsilon \epsilon_0 \omega R_H^6, \tag{21}$$

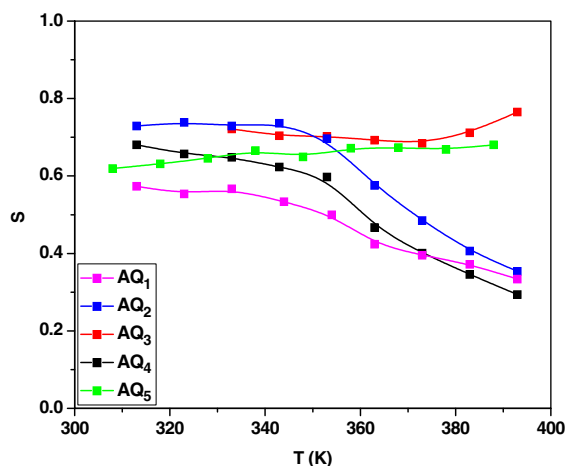


Fig. 12. Plot of the frequency exponent (S) vs. T for ligands (AQ_x).

where N is the density of a pair of sites. The hopping length, R_H , is expressed as:

$$R_H = \frac{ne^2}{\pi\epsilon\epsilon_0} \left[w_m - k_B T \ln \frac{1}{\omega\tau_0} \right]. \quad (22)$$

The frequency exponent (S) in this model is given by the equation [36]:

$$S = 1 - \frac{6k_B T}{\left[w_m - k_B T \ln \left(\frac{1}{\omega\tau_0} \right) \right]}. \quad (23)$$

First approximation to Eq. (23) gave the expression:

$$S = 1 - \frac{6K_B T}{W_m}. \quad (24)$$

In CBH model, the electrons in charged defect states, hop over the Coulomb barrier whose height (W) is given by the equation [36]:

$$W = W_m + \frac{8e^2}{\epsilon\epsilon_0 R}, \quad (25)$$

where W_m is the maximum barrier height (the energy required moving the electron from a site to infinity), R is the distance between hopping

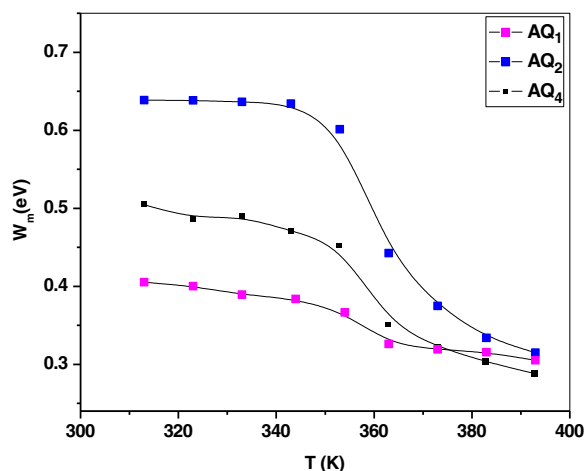


Fig. 13. The maximum barrier height (W_m), as a function of temperature, for the ligands AQ_1 , AQ_2 and AQ_4 .

states. The maximum barrier height (W_m) as a function of temperature for AQ_1 , AQ_2 and AQ_4 is plotted in Fig. 13. The value W_m decreases with increasing temperature for AQ_1 , AQ_2 and AQ_4 .

4. Conclusion

5-(2-Aryldiazanyl)quinolin-8-ol (AQ_x) ligands are synthesized by azo coupling reaction. The alternating current conductivity (σ_{ac}) and dielectric properties of AQ_x are investigated in the frequency range 10^2 – 10^5 Hz. The real and imaginary parts of the dielectric constant ϵ_i and ϵ_r increase with increasing the temperature and decrease with increasing frequency for all AQ_x . The calculated values of σ_{ac} increase with increasing frequencies for all AQ_x . The correlated barrier hopping (CBH) is the dominant conduction mechanism for ligands AQ_1 , AQ_2 and AQ_4 , while for ligands AQ_3 and AQ_5 the small polaron tunneling (SPT) is the dominant conduction mechanism. The probable electronic transitions were found to be direct forbidden transition for all ligands and indirect allowed transition for the AQ_1 and AQ_4 ligands. The optical values of energy gap (E_g) for all derivatives were in the range 1.34–2.26 eV for direct transitions and 1.47–1.69 eV for indirect transitions. It was found that the change of substituents affects the thermal properties, dielectrical properties, ac conductivity, optical properties and the values of the thermal activation energy of AQ_x .

Appendix A. Supplementary data

Supplementary data to this article can be found online at <http://dx.doi.org/10.1016/j.molliq.2015.07.050>.

References

- [1] A.Z. El-Sonbati, M.A. Diab, A.A. El-Bindary, Sh.M. Morgan, *Inorg. Chim. Acta* 404 (2013) 175–187.
- [2] M.A. Diab, A.Z. El-Sonbati, A.A. El-Bindary, G.G. Mohamed, Sh.M. Morgan, *Res. Chem. Intermed.* (2015) <http://dx.doi.org/10.1007/s11164-015-1946-0>.
- [3] J. Koh, A.J. Greaves, *Dyes Pigments* 50 (2001) 13–19.
- [4] K. Maho, T. Shintaro, K. Yutaka, W. Kazuo, N. Toshiyuki, T. Moshiko, *Jpn. J. Appl. Phys.* 42 (2013) 1068–1075.
- [5] D.W. Rangnekar, V.R. Kanetkar, J.V. Malanker, G.S. Shankarling, *Indian J. Fibre Text Res.* 24 (1999) 142–1944.
- [6] A.S.A. Zidan, *J. Therm. Anal. Calorim.* 68 (2002) 1045–1059.
- [7] A.F. Shoaib, A.A. El-Bindary, A.Z. El-Sonbati, R.M. Younes, *Spectrochim. Acta A* 57 (2001) 1683–1691.
- [8] A.K.A. Hadi, *Pol. J. Chem.* 68 (1994) 803–806.
- [9] N.A. El-Ghamaz, M.A. Diab, A.Z. El-Sonbati, O.L. Salem, *Spectrochim. Acta A* 83 (2011) 61–66.
- [10] N.A. El-Ghamaz, M.A. Diab, A.A. El-Bindary, A.Z. El-Sonbati, S.G. Nozha, *Spectrochim. Acta A* 143 (2015) 200–212.
- [11] M. Saçmacı, H.K. Çavuş, H. Arı, R. Şahingöz, T. Özpozan, *Spectrochim. Acta A* 97 (2012) 88–99.
- [12] N.A. El-Ghamaz, E.M. El-Menyawy, M.A. Diab, A.A. El-Bindary, A.Z. El-Sonbati, S.G. Nozha, *Solid State Sci.* 30 (2014) 44–54.
- [13] N.A. El-Ghamaz, H.M. El-Mallah, A.Z. El-Sonbati, M.A. Diab, A.A. El-Bindary, A.M. Barakat, *Solid State Sci.* 22 (2013) 56–64.
- [14] H.M. Zeyada, N.A. El-Ghamaz, E.A. Gamal, *Curr. Appl. Phys.* 13 (2013) 1960–1966.
- [15] A.Z. El-Sonbati, A.A. El-Bindary, A.F. Shoaib, R.M. Younes, *Chem. Pharm. Bull.* 49 (2001) 1308–1313.
- [16] A.Z. El-Sonbati, A.A. El-Bindary, *Pol. J. Chem.* 74 (2000) 621–630.
- [17] N.A. El-Ghamaz, M.A. Diab, A.A. El-Bindary, A.Z. El-Sonbati, H.A. Seyam, *Mater. Sci. Semicond. Process.* 27 (2014) 521–531.
- [18] H.M. Shabana, *Polym. Test.* 23 (2004) 695–702.
- [19] R. Shirley, *The CRYSPFIRE System for Automatic Powder Indexing: User's Manual*, the Lattice Press, Guildford, Surrey GU2 7NL, England, 2000.
- [20] A.Z. El-Sonbati, M.A. Diab, A.A. El-Bindary, A.M. Eldesoky, Sh.M. Morgan, *Spectrochim. Acta A* 135 (2015) 774–791.
- [21] M.M. Ghoneim, A.Z. El-Sonbati, A.A. El-Bindary, M.A. Diab, L.S. Serag, *Spectrochim. Acta A* 140 (2015) 111–131.
- [22] A.Z. El-Sonbati, A.A. Belal, S.I. El-Wakeel, M.A. Hussien, *Spectrochim. Acta A* 60 (2004) 965–972.
- [23] A.T. Mubarak, A.Z. El-Sonbati, S.M. Ahmed, *J. Coord. Chem.* 60 (2007) 1877–1890.
- [24] A.Z. El-Sonbati, R.M. Issa, A.M. Abd El-Gawad, *Spectrochim. Acta A* 68 (2007) 134–138.
- [25] M.A. Hepler, T.L. Riechel, *Inorg. Chim. Acta* 54 (1981) 255–257.
- [26] A.N. Specca, L.L. Pyhewski, N.M. Karayannis, C. Owens, *J. Inorg. Nucl. Chem.* 36 (1974) 3751–3759.
- [27] A.Z. El-Sonbati, M.A. Diab, A.A. El-Bindary, G.G. Mohamed, Sh.M. Morgan, *Inorg. Chim. Acta* 430 (2015) 96–107.

- [28] C. Hammond, *The Basics of Crystallography and Diffraction*, 3rd ed. Oxford University Press, 2009.
- [29] H.M. Zidan, N.A. El-Ghamaz, A.M. Abdelghany, A. Lottfy, *Res. J. Pharm. Biol. Chem. Sci.* 4 (2015) 985–1000.
- [30] H. Gao, Q. Li, Y. Dai, F. Luo, H.X. Zhang, *Corros. Sci.* 52 (2010) 1603–1609.
- [31] M.P. Singh, C.S. Thakur, K. Shalini, S. Banerjee, N. Bhat, S.A. Shivashankar, *J. Appl. Phys.* 96 (2004) 5631–5638.
- [32] M.M. Khedr Abo-Hassan, M.R. Muhamad, S. Radhakrishna, *Thin Solid Films*, 491 (2005) 117–122.
- [33] R. Tsu, P. Menna, A.H. Mahan, *Sol. Cells* 21 (1987) 189–194.
- [34] L. Leontie, R. Danac, *Scr. Mater.* 54 (2006) 175–179.
- [35] I.G. Hill, A. Kahn, Z.G. Soos, R.A. Pascal Jr., *Chem. Phys. Lett.* 327 (2000) 181–188.
- [36] N.A. El-Ghamaz, A.Z. El-Sonbati, M.A. Diab, A.A. El-Bindary, M.K. Awad, Sh.M. Morgan, *Mater. Sci. Semicond. Process.* 19 (2014) 150–162.
- [37] N.A. El-Ghamaz, A.Z. El-Sonbati, M.A. Diab, A.A. El-Bindary, Sh.M. Morgan, *Mater. Res. Bull.* 65 (2015) 293–301.
- [38] N.A. El-Ghamaz, A.Z. El-Sonbati, M.A. Diab, A.A. El-Bindary, G.G. Mohamed, Sh.M. Morgan, *Spectrochim. Acta A* 147 (2015) 200–211.
- [39] S.R. Elliott, *Adv. Phys.* 36 (1987) 135–217.
- [40] A.R. Long, *Adv. Phys.* 31 (1982) 553–637.